Desert Dust Air Mass Mapping in the Western Sahara, Using Particle Properties Derived From Space-based Multi-angle Imaging

Ralph Kahn[1], Andreas Petzold[2], Manfred Wendisch[3], Eike Bierwirth[3], Tilman Dinter[4], Marcus Fiebig[5], Peter Knippertz[3], Detlef Müller[6], Alexander Schladitz[6], Wolfgang von Hoyningen-Huene[4]

[1] NASA Goddard Space Flight Center, Greenbelt MD 20771 USA
[2] Institute for Atmospheric Physics, German Aerospace Center (DLR), Wessling, Germany
[3] Institute for Atmospheric Physics, Johannes Gutenberg-University Mainz, Germany
[4] Institute of Environmental Physics, University of Bremen, Germany
[5] Department of Atmospheric and Climate Research, Norwegian Institute for Air Research, Kjeller, Norway
[6] Leibniz Institute for Tropospheric Research, Leipzig, Germany

Tellus

SAMUM Special Issue

Submitted: March 2008

Keywords: desert dust, aerosol remote sensing, multi-angle imaging, SAMUM campaign, aerosol air mass types

Abstract

Coincident observations made over the Moroccan desert during the SAhara Mineral dUst experiMent (SAMUM) 2006 field campaign are used both to validate aerosol amount and type retrieved from Multi-angle Imaging SpectroRadiometer (MISR) observations, and to place the sub-orbital aerosol measurements into the satellite's larger regional context. On three moderately dusty days for which coincident observations were made, MISR mid-visible aerosol optical thickness (AOT) agrees with field measurements point-by-point to within 0.05 to 0.1. This is about as well as can be expected given spatial sampling differences; the space-based observations capture AOT trends and variability over an extended region. The field data also validate MISR's ability to distinguish and to map aerosol air masses, from the combination of retrieved constraints on particle size, shape, and single-scattering albedo. For the three study days, the satellite observations (a) highlight regional gradients in the mix of dust and background spherical particles, (b) identify a dust plume most likely part of a density flow, and (c) show an air mass containing a higher proportion of small, spherical particles than the surroundings, that appears to be aerosol pollution transported from several thousand kilometers away.

1. Introduction

Satellite instruments such as the Multi-angle Imaging SpectroRadiometer (MISR) routinely produce global maps reporting aerosol amount and type. However, much remains to be learned about the accuracy of these products, and about how they can be used for regional studies that require both the extensive coverage satellites provide, as well as a level-of-detail obtainable only from sub-orbital platforms.

During the SAhara Mineral dUst experiMent (SAMUM) [*Heintzenberg et al.,* this issue] in May and June 2006, coincident surface, airborne, and satellite measurements of the nearly pure dust aerosol in the skies around Ouarzazate and Zagora, Morocco were collected. This region, at the western edge of Saharan dust sources, was targeted due to the trans-continental environmental impact these aerosols have, an observation first made at the advent of the satellite era [e.g., *Prospero et al.,* 1999].

The MISR team participated actively in SAMUM field operations; this paper provides a summary of our initial scientific results. MISR, which flies aboard the NASA Earth Observing System's Terra satellite [http://www-misr.jpl.nasa.gov], is especially well suited to study aerosols in the desert environment on ten-to-hundred-kilometer scales. MISR makes near-simultaneous measurements at nine view-angles spread out in the forward and aft directions along the flight path, at ±70.5°, ±60.0°, ±45.6°, ±26.1°, and nadir, in each of four spectral bands centered at 446, 558, 672, and 866 nm [*Diner et al.*, 1998].

With these observations, the instrument systematically covers a range of air-mass factors from one to three, providing greater sensitivity to aerosol optical thickness (AOT) than single-view measurements, over land in general [*Abdou et al.,* 2005; *Kahn et al.,* 2005] and especially over bright surfaces such as desert [*Martonchik et al.*, 2004]. In mid-latitudes, MISR samples

scattering angles extending from about 60° to 160°, making it possible to distinguish spherical particles, such as aerosol pollution, from non-spherical desert dust [*Kalashnikova and Kahn*, 2006; *Kahn et al.*, 1997], and to derive some information about particle size and single-scattering albedo (SSA) [*Chen et al.*, 2008; *Kahn et al.*, 1998]. Note that the MISR spectral range provides sensitivity to particle properties for aerosol up to about 2.5 μm in diameter ($PM_{2.5}$), but is insensitive to the properties of larger particles, which is a limitation in desert applications, especially near sources. MISR views nearly the entire Earth about once per week, with spatial sampling of 275 m to 1.1 km, depending on channel and instrument operating mode. The MISR Standard Aerosol Product is reported over 17.6 km regions [*Martonchik et al.*, 1998; 2002].

The primary motivations for MISR team participation in SAMUM are: (a) to quantify MISR's ability to retrieve AOT and mineral dust properties over bright desert surfaces, and (b) to contribute to the campaign data set MISR regional AOT and aerosol air mass type maps. The maps provide context for the more detailed but less extensive measurements made by the aircraft and ground-based platforms. We present here both initial validation results and regional maps for three Golden Days, 19 May, 28 May, and 04 June 2006, during which aircraft and surface data were acquired coincident with the MISR overpasses. These days happen to fall within each of the three SAMUM dusty periods identified with aircraft data [*Petzold et al.*, this issue]. At the Tinfou surface station near Zagora, high dust concentrations were recorded on 19 and 28 May [*Schladitz et al.*, this issue], and on 04 June, dust-laden density current outflows were documented in Meteosat images and surface meteorological station data [*Knippertz et al.* 2007].

The following sections report the MISR observations on each day, present maps of retrieved AOT and particle properties, and offer a preliminary assessment of MISR Standard Aerosol retrieval results in light of near-coincident field data. A summary and conclusions are provided at the end.

2. Aerosol Air Mass Analyses

A brief review of the aerosol amount and property constraints produced by MISR over the study region, comparing, to the extent possible, values and trends with near-simultaneous field data acquired during SAMUM, reveals the contributions both the satellite and sub-orbital data make to environmental characterization. Although MISR did not image a major dust storm in the study area during this campaign, mid-visible AOT $\gtrsim$0.5 from regional dust storms, as well as gradients of airborne dust and spherical background particles, were observed at ~10 to ~100 km scales on all three days.

2.1. 19 May 2006

This section presents results for the first of three Golden Days. It includes a summary of particle properties derived from aircraft and surface observations that are used to compare with MISR-retrieved values in subsequent sections as well.

2.1.1 Retrieved Aerosol Amount and Type Patterns

Figure 1 gives a point-to-point comparison between MISR and surface-retrieved AOT at the Ouarzate and Tinfou study sites on 19 May 2006. MISR Standard Aerosol mid-visible AOT

retrievals at 17.6 km spatial resolution in the vicinity of Ouarzazate were clustered between 0.35 and 0.45. The AERONET retrievals [*Holben et al.,* 1998] show AOT in this spectral range increasing from about 0.36 to 0.43 over the morning hours leading up to the overpass, and leveling off at about 0.45 shortly thereafter. This amounts to close agreement between the surface and MISR AOT measurements, given the differences in spatial and temporal sampling. Similarly, the sun photometer at Tinfou registered mid-visible AOTs slightly higher than at Ouarzazate.

A comprehensive view of AOT and optical properties for the MISR overpass is given in Figure 2. The MISR retrievals illustrated in Figure 2a show greater AOT spatial variability in the vicinity of Tinfou than at Ouarzazate, and corresponding temporal variability is observed as occasional peaks in the Tinfou sun photometer AOT time series (Figure 1c). The observations show a consistent envelope of MISR AOT values encompassing the range observed from the surface, suggesting that local dust sources may have been active during the late morning. This interpretation is supported by local meteorological conditions. 19 May was a day on which the mean wind speed was fairly low, but dry convective dust plume activity that could cause this small-scale variability was reported at Ourazazate some time between 10:00 and 12:00 UTC (see Fig. 9 of *Ansmann et al.,* this issue). The 11:11 UTC MISR overpass time might have occurred near the start of local plume activity.

Mid-visible AOT increases from between 0.4 and 0.5 in the prime study region to over 1.0 about 350 km to the SSW (Figure 2a). Panels b-d of Figure 2 show the retrieved Ångström exponent, SSA, and fraction AOT spherical (which is the fraction of the total-column mid-visible AOT that the algorithm did *not* assign to non-spherical dust components). These particle microphysical properties all diminish as AOT increases on the regional scale, suggesting larger, non-spherical, dust-like particles are more abundant in this direction. In particular, the dust contribution to mid-visible AOT increases from about 40% to as much as 70%, as the total column AOT increases.

HYSPLIT back trajectories [*Draxler and Rolph*, 2003] for Ouarzazate and Tinfou indicate that the entire region was under the influence of a high-pressure system centered over north-central Algeria, causing air at all levels to sweep across central Algeria from east to west, arriving at the study sites from the ESE [not shown, but similar to the situation two days earlier given in Fig. 2b of *Knippertz et al.,* this issue]. This picture is consistent with the fairly uniform air mass derived by MISR for the ~200 km N-S region that includes the study sites themselves. Further, animations of the Meteosat Second Generation (MSG) dust product [*Schepanski et al.*, 2007] suggest that the higher regional AOT observed this day over western Algeria by MISR originated primarily from two local sources near the western edge of the Tademaït Plateau on 18 May [see *Heinold et al.,* this issue, Fig. 1h].

2.1.2 Particle Microphysical Property Validation

SAMUM field measurements included aircraft and ground-based aerosol and surface optical property measurements on all three MISR Golden Days. We use these as "ground truth" against which to compare with MISR particle property retrieval results. Generally, the field measurements detected two components, medium non-spherical, relatively bright dust and small, spherical, more absorbing background particles, which may be transported aerosol pollution or smoke, in varying proportions.

Specifically, near-surface aerosol optical property observations made at Tinfou found a coarse mode component having a number-weighted median diameter of about 0.6 μm and a volume-weighted median diameter between 2 and 3 μm, for periods covering both the 19 and 28 May MISR events [*Schladitz et al.* this issue]. This component was associated with mineral dust. On 27-28 May, when dust dominated the aerosol load, the SSA was about 0.96±0.02 at 530 nm and 0.98±0.01 at 630 nm wavelengths. A spherical fine mode, having median diameter around 0.07-0.09, μm was also detected. On 29-30 May, when this component contributed a larger fraction to the total optical depth than on other days (though there were no coincident MISR observations), the effective SSA was about 0.91±0.02 at 530 nm and 0.93±0.01 at 630 nm wavelengths [*Schladitz et al.* this issue].

Similar conclusions about particle microphysical properties were reached based on near-coincident airborne measurements of aerosol layers between about 1.5 and 5 km above sea level (ASL), except that mid-visible SSA values below 0.8 were recorded from the aircraft [*Otto et al,* this issue; *Petzold et al.*, this issue]. These values are quite low for aged aerosols, but their difference compared to surface measurements is not entirely surprising, since initially low-SSA transported aerosol pollution is likely to be concentrated in isolated layers aloft. In addition, *Otto et al.* [this issue, Figure 2c] find the relative humidity (RH) at these elevations is below 45% from radiosonde measurements nearly coincident with the MISR overpass on 19 May. If RH in the aerosol layers remained low during transport, hydration and chemical aging, that dominate aerosol evolution in more humid environments, may not be effective at increasing particle SSA here.

From the aggregate of field observations described in the references above, including particle indices of refraction, size distributions, size distribution discrepancies among different measurement techniques, hygroscopicity, and composition, it was also deduced that the component size distributions and coarse-mode microphysical properties were fairly stable over the entire SAMUM measurement period. The coarse mode optical properties overall are similar to those of weakly absorbing grains modeled by *Kalashnikova et al.* [2005], and used in the Standard MISR aerosol retrieval algorithm as "medium grains" (Table 1).

The MISR algorithm uses a set of absolute criteria to decide which aerosol mixtures, from a list of candidates that is applied globally, provide acceptable matches to the observed radiances [*Martonchik et al.,* 1998; *Kahn et al.,* 2001]. Multiple mixtures may pass the acceptance tests, and the range of properties gives some indication of the constraints provided by the MISR radiances. For the Standard algorithm version used here (V19), this list contains 74 mixtures (Table 2), comprised of up to three of eight components (Table 1). There are three groupings of bi-modal, spherical, non-absorbing particles; each group has a coarse mode of radius 2.80 μm, combined with a fine mode of radius 0.06, 0.12, or 0.26 μm, in ten increments of varying proportions. These are followed in Table 2 by two groups of ten mixtures each, for which the fine mode is an absorbing, spherical particle of radius 0.12, having mid-visible SSA 0.90 and 0.80, respectively. The remaining 24 mixtures are bi- and tri-modal distributions that include medium or medium + coarse mode dust analogs.

On 19 May, for retrieval regions surrounding the Ouarzazate surface station, the MISR algorithm preferentially selected mixtures containing about 60% mid-visible optical depth dust (e.g.,

Mixtures 58, 63, and 64 in Table 2). The second component is primarily medium, spherical, non-absorbing particles, an outcome consistent with field measurements. This is a satisfactory result for identifying aerosol air mass type: dust, plus a fine-mode spherical component. However, looking in more detail at particle size and SSA, the retrieved spherical component, having number-weighted mean geometric radius of 0.12 μm, is both less absorbing and significantly larger than the spherical fine mode observed in the field. But note that the 0.12 μm particle is the only spherical component in mixtures containing both spherical and non-spherical particles allowed by the Version 19 Standard algorithm (Table 2). For fixed AOT, larger particles having the same SSA scatter less light, so to some extent the MISR algorithm may substitute larger, brighter particles for the smaller, darker ones observed *in situ*, still obtain very good AOT agreement, and still preserve the mixed spherical + non-spherical aerosol air mass category.

At most locations in the vicinity of Ouarzazate, on this relatively high AOT day, the MISR algorithm accepted no more than two or three dust-containing mixtures, as described above. In a few places, other mixtures that met the acceptance criteria, though not the lowest-residual (best-fitting) mixtures, contain up to 30% of the very large, spherical, non-absorbing particles (Mixtures 52 and 55 in Table 2). Here the algorithm may be substituting large spherical particles for a super-μm mineral dust component, since the available optical analog (Particle 21 in Table 1), derived using a spheroidal approximation, may not adequately represent the natural particles [*Kalashnikova et al.*, 2005].

There are also several sites at which eight or more mixtures passed, including some containing only medium spherical particles. When so many mixtures having different microphysical properties are retrieved, it is an indication that the particle property retrieval itself is not well constrained. If this occurs because the total column AOT is low, the AOT retrieval does not depend heavily on particle properties, and may still be robust [*Kahn et al.*, 1998; 2005]. Other possible causes, likely in this case, are inadequate surface or aerosol optical models, or varying aerosol amount or properties within the retrieval region; these contingencies violate fundamental assumptions of the algorithm. MISR results for Tinfou are similar, with dust + a fine-mode spherical component comprising the lowest residual mixtures selected, though there are more cases where multiple mixtures of varying properties passes, most likely reflecting the greater small-scale aerosol loading variability seen in Figure 2.

In summary, within the limitations of the algorithm mixture table, the MISR retrievals found bi-modal distributions containing significant dust, combined with a fine-mode, spherical component, in rough agreement with field observations, and adequate to distinguish aerosol air mass types. However, a lack of mixtures containing small, spherical, absorbing particles combined with dust, and suspected limitations of the optical model used for super-μm sized mineral dust, limit the degree to which the satellite-derived particle properties could match those observed directly. One reason for performing particle property field validation is to identify limitations in the current Standard algorithm, such as those found here. The MISR Research Aerosol Retrieval algorithm, with which a vastly wider range of aerosol components and mixtures can be explored than with the Standard algorithm, is the key tool for such investigations [e.g., *Kahn et al.*, 2001; *Kalashnikova and Kahn*, 2006; *Chen et al.*, 2008]. This is beyond the scope of the current paper, but is the subject of continuing work aimed at refining the Standard algorithm component and mixture tables, and quantifying the sensitivity of the upgraded algorithm.

2.2. 28 May 2006

A point comparison of mid-visible AOT at the prime study sites for the 28 May event is given in Figure 3. On this day there is a definite gradient, reflected in both the satellite and surface measurements, with AOT 0.1 to 0.15 higher at Tinfou. The MISR regional view of AOT and particle properties given in Figure 4 shows this gradient in a larger context.
AOT is more variable in the study region than it was on 19 May, and what appear to be local sources show up as patches of higher AOT one or two 17.6 km retrieval regions in size, in both the plains south of Ouarzazate and the Zagora basin farther east. On the ~100 km scale, a weak gradient in retrieved particle properties is observed, with somewhat lower Ångström exponent, higher SSA, and no clear trend in fraction AOT spherical, extending at least 200 km to the NE from Tinfou.

Based on HYSPLIT back trajectories, Ouarzazate and Tinfou are in the same regional air flow at all levels; the near-surface (0.5 km) air comes due west from central Algeria, whereas the mid-level (1.5 km) flow is due north from western Algeria, and the upper level (2.5 km) air is advected from the W Sahara, through Mauritania, Mali, and Algeria into W Morocco [not shown, but see *Schladitz et al.* this issue, Fig. 8c]. The similarity of regional wind patterns at the ground stations supports the idea that the observed AOT gradient between Ouarzazate and Tinfou is due to one or more local sources near Tinfou rather than regional-scale activity, though orographic blocking or other topographic effects not reproduced on the scale of the model back trajectories could also be contributing to the observed differences.

As on 19 May, MISR particle property retrievals favor the ~ 60% dust + fine-mode spherical mixtures available in the algorithm (especially Mixtures 55, 57, 58, and 63 in Table 2), and results at Ouarzazate are more tightly constrained than those in the Zagora region. The 28 May event falls during Period 2 of the SAMUM campaign; detailed analysis shows hardly any aerosol compositional differences compared to Period 1 (which included 19 May) [*Petzold et al.*, this issue; *Schaditz et al.*, this issue]. As expected, MISR-retrieved aerosol microphysical properties over the study region for these two events are indistinguishable.

2.3. 04 June 2006

Mid-visible AOT for 04 June follows a pattern similar to the other days, with values around 0.5, and Tinfou slightly higher than Ouarzazate at MISR overpass time (Figure 5), even though on this day, AOT over Tinfou decreases during the morning hours prior to overpass. Particle property retrieval results at the two prime study sites also reproduce those of the previous Golden Days. But the regional view in Figure 6 reveals several new features of interest. A high AOT region of large, bright, largely non-spherical particles appears about 300 km south of Tinfou. This we identify as a dust storm. The dust is likely the remnant of a plume created the previous day by a large density current that formed along the slopes of the High Atlas mountains, as precipitation evaporated above the ground, cooling the associated air mass [*Knippertz et al.* 2007, Fig. 9b]. The front passed Tinfou in the early morning hours of 04 June, and by MISR overpass time (11:11 UTC), at the estimated speed of ~ 8 m/s, it would have traveled between

about 200 and 300 km farther south, to the approximate location of the feature observed in Figure 6. Other satellite observations also show the edge of an airborne dust cloud near the MISR-observed location, though at different times during this day [*Heinold et al.*, this issue, Figure 2, column 3]. In general, geostationary instruments such as the Meteosat imager are far more effective at tracking the motions of such storms [e.g., *Knippertz et al.*, 2007] than relatively narrow-swath instruments on polar orbiting satellites, but MISR does provide additional information: at its thickest, the mid-visible AOT in the observed part of the plume is close to 1.3, and roughly 50% of this is attributed to non-spherical particles.

A more subtle feature appears to the south and east of Ouarzazate, just south and west of Tinfou, that seems to be a relative enhancement of small-medium, spherical, very bright particles (outlined in Figure 6b). This may simply be a region of reduced dust concentration, as the total column AOT is ~0.35, compared to about 0.5 for the lower SSA, lower Ångström Exponent areas to the south and east. The fraction AOT spherical within the feature is about 0.8, whereas in the surroundings, it is near 0.5, implying a spherical particle AOT of 0.28 and 0.25, respectively. This represents only a marginally higher column abundance of small particles, at the limit of MISR detectability for such relative distinctions.

Although no field measurements were taken near the core of the MISR feature, SAMUM data shed some light on the likely interpretation. Particle size distributions measured *in situ* between 10:24-10:31 UTC over Ouarzazate show a markedly enhanced fine-mode aerosol concentration at 1.9 km ASL [*Heinold et al.*, this issue, Figure 10e]. Airborne lidar over the site exhibits a backscatter peak less than an hour earlier between 2.5 and 3.5 km, identified as dust, and additional peaks between 1.5 and 2 km, and around 4 km [*Esselborn et al.*, this issue]. Three-day HYSPLIT back trajectories for the two prime study sites and a location near the center of the small-particle feature, evaluated at about the peak of each layer observed over Ouarzazate, are plotted in Figure 7. Of these, the trajectories culminating at 1.8 km ASL above the feature location and over Tinfou cross population centers in northern Algeria from which a layer of small, spherical aerosol pollution particles could have originated. But the evidence in this case is only circumstantial. The challenge of obtaining strong validation data over parts of the MISR swath away from the immediate study region illustrate the complementary nature of satellite and sub-orbital data, and highlight the value of assessing MISR aerosol retrieval quality, where possible, though field campaigns such as SAMUM.

3. Summary and Conclusions

This paper takes the initial steps toward validating MISR's ability to retrieve aerosol optical and microphysical properties of desert dust and related air mass types over bright desert surfaces, using near-coincident field data acquired during the SAMUM campaign of 2006. It also provides regional maps of aerosol amount and properties derived with the MISR Standard aerosol algorithm (Version 19).

MISR mid-visible AOT agrees point-by-point with available validation data within 0.05 to 0.1, about as well as can be expected given spatial sampling differences. The satellite observations capture AOT trends and variability over extended regions, providing context for more detailed sub-orbital measurements.

The field data are also used to probe the limits of MISR's ability to distinguish and to map aerosol air masses, from the combination of retrieved constraints on particle size, shape, and single-scattering albedo. For the three SAMUM Golden Days, 19 and 28 May and 04 June 2006, the satellite observations highlight regional gradients in the mix of dust and background spherical particles, identify a dust plume that is most likely part of a density flow, and show an air mass containing a higher proportion than the surroundings of small, spherical particles. This air mass appears to be aerosol pollution transported from several thousand kilometers away.

Aggregating particle properties into aerosol air mass types offers a more robust quantity than do the retrieved particle microphysical properties individually. We identified a lack of small, spherical, absorbing particles in the MISR algorithm's complement of bi-modal mixtures containing mineral dust, and found evidence supporting earlier indications that the spheroidal coarse-mode dust optical model currently used is not optimal for multi-angle retrievals. A next step in refining the MISR aerosol algorithm and assessing its quality involves exploring quantitatively the ranges of aerosol components and mixtures to which MISR is sensitive, using cases where the answer is known from direct measurements. This is one value of the SAMUM Golden Day observations, and is the subject of continuing work.

The MISR data set for the SAMUM Campaign is available through a dedicated web site at the NASA Langley Atmospheric Sciences Data Center:
http://eosweb.larc.nasa.gov/PRODOCS/misr/samum/table_samum.html

Acknowledgments

We thank our colleagues on the Jet Propulsion Laboratory's MISR instrument team and at the NASA Langley Research Center's Atmospheric Sciences Data Center for their roles in producing the MISR data sets, and A. Ansmann for supporting the Ouarzazate AERONET station. R. Kahn thanks Jost Heintzenberg and colleagues for the invitation to participate in the SAMUM Campaign, and the SAMUM Research Community for their hospitality. The work of R. Kahn is supported in part by NASA's Climate and Radiation Research and Analysis Program, under H. Maring, NASA's Atmospheric Composition Program under R. Halthore, and the EOS-MISR instrument project.

References

Abdou, W.A., D.J. Diner, J.V. Martonchik, C.J. Bruegge, R.A. Kahn, B.J. Gaitley, K.A. Crean, L.A. Remer, and B. Holben, 2005, Comparison of coincident MISR and MODIS aerosol optical depths over land and ocean scenes containing AERONET sites, *J. Geophys. Res.*, doi:10.1029/2004JD004693.

Ansmann, A., Tesche, M., Knippertz, P., Bierwirth, E., Althausen, D., Müller, D., and Schulz, O., 2008. Vertical profiling of convective dust plumes in southern Morocco during SAMUM. Vertical profiling of convective dust plumes in southern Morocco during SAMUM. *Tellus*, this issue.

Chen, W-T., R. Kahn, W-H. Li, and J. Seinfeld, 2008, Sensitivity of multi-angle imaging to optical and microphysical properties of biomass burning particles, *J. Geophys. Res.*, in press.

Diner, D.J., J.C. Beckert, T.H. Reilly, C.J. Bruegge, J.E. Conel, R. Kahn, J.V. Martonchik, T.P. Ackerman, R. Davies, S.A.W. Gerstl, H.R. Gordon, J-P. Muller, R. Myneni, R.J. Sellers, B. Pinty, and M.M. Verstraete, Multiangle Imaging SptectrRadiometer (MISR) description and experiment overview, IEEE Trans. Geosci. Remt. Sensing 36, 1072-1087, (1998).

Dinter, T., W. von Hoyningen-Huene, J.P. Burrows, A. Kokhanovsky, E. Bierwirth, M. Wendisch, D. Muller, R. Kahn, and M. Diouri, 2008. Regional patterns of satellite retrievals of aerosol optical depths of desert dust during SAMUM campaign with MERIS and validation. *Tellus*, this issue.

Draxler, R. R., and G. D. Rolph (2003), HYSPLIT (HYbrid Single-Particle Lagrangian Integrated Trajectory) Model access via the NOAA ARL READY Website, NOAA Air Resour. Lab., Silver Spring, Md. (Available at http://www.arl.noaa.gov/ready/hysplit4.html).

Esselborn, M., M. Wirth, A. Fix, B. Weinzierl, K. Rasp, M. Tesche, and A. Petzold, 2008. Spatial distribution and optical properties of Saharan dust observed by airborne high spectral resolution lidar during SAMUM 2006. *Tellus*, this issue.

Heinold, B., I. Tegen, P. Knippertz, B. Laurent, K. Schepanski, D. Müller, A. Petzold, M. Esselborn, B. Weinzierl, K. Kandler, A. Schladitz, A. Ansmann, D. Althausen, and M. Teische, 2008. Regional Saharan dust modeling during the SAMUM 2006 campaign. *Tellus*, this issue.

Heintzenberg, J., 2008: The SAMUM-1 experiment over Southern Morocco: Overview and introduction. *Tellus*, this issue.

Holben, B.N., et al., 1998, AERONET – A federated instrument network and data archive for aerosol characterization, Remote Sens. Environ. 66 1-16.

Kahn, R., R. West, D. McDonald, B. Rheingans, and M.I. Mishchenko, 1997. "Sensitivity of Multi-angle remote sensing observations to aerosol sphericity ", J. Geophys. Res., 102, 16861-16870.

Kahn, R., P. Banerjee, D. McDonald, and D. Diner, 1998. "Sensitivity of Multiangle imaging to Aerosol Optical Depth, and to Pure-Particle Size Distribution and Composition Over Ocean ", J. Geophys. Res. 103, 32,195-32,213.

Kahn, R., P. Banerjee, and D. McDonald, 2001. The Sensitivity of Multiangle Imaging to Natural Mixtures of Aerosols Over Ocean, *J. Geophys. Res.106* 18219-18238.

Kahn, R., B. Gaitley, J. Martonchik, D. Diner, K. Crean, and B. Holben, 2005, MISR global aerosol optical depth validation based on two years of coincident AERONET observations, *J. Geophys. Res., doi:10:1029/2004JD004706.*

Kalashnikova, O.V., R. Kahn, I.N. Sokolik, and W-H. Li, 2005, The ability of multi-angle remote sensing observations to identify and distinguish mineral dust types: Part 1. Optical models and retrievals of optically thick plumes, *J. Geophys. Res.*,doi: 10.1029/2004JD004550.

Kalashnikova, O.V. and R.A. Kahn, 2006. The ability of multi-angle remote sensing observations to identify and distinguish mineral dust types: Part 2. Sensitivity data analysis, *J. Geophys. Res.*, 111, D11207, doi:10.1029/2005JD006756.

Knippertz, P., Deutscher, C., Kandler, K., Müller, T., Schulz, O. and Schütz, L. 2007. Dust mobilization due to density currents in the Atlas region: Observations from the SAMUM 2006 field campaign. *J. Geophys. Res.* **112,** doi:10.1029/2007JD008774.

Knippertz, P., A. Ansmann, D. Althausen, D. Müller, M. Tesche, E. Bierwirth, T. Müller, T. Dinter, W. Von Hoyningen-Huene, K. Schepanski, M. Wendisch, B. Heinold, K. Kandler, A. Petzold, L. Schütz, and I. Tegen, 2008. Dust mobilization and transport in the northern Sahara during SAMUM 2006 – A meteorological overview. *Tellus*, this issue.

Martonchik, J.V., D.J. Diner, R.A. Kahn, B.J. Gaitley, and B.N. Holben, 2004, Comparison of MISR and AERONET aerosol optical depths over desert sites, *Geophys. Res. Let. 31,* doi:10.1029/2004GL019807.

Martonchik, J.V., D.J. Diner, K.A. Crean and M.A. Bull, 2002. Regional Aerosol Retrieval Results From MISR. IEEE Trans. Geosci. Remote Sens., 40:1520-1531.

Martonchik, J.V., D.J. Diner, R. Kahn, M.M. Verstraete, B. Pinty, H.R. Gordon, and T.P. Ackerman, 1998. Techniques for the Retrieval of aerosol properties over land ocean using multiangle data, IEEE Trans. Geosci. Remt. Sensing 36, 1212-1227.

Otto, S., T. Trautmann, K. Kandler, E. Bierwirth, and M. Wendisch, 2008. Radiative closure of a Saharan dust plume observed during SAMUM. *Tellus*, this issue.

Petzold, A., K. Rasp, B. Weinzierl, M. Esselborn, T. Hamburger, G. Ehret, A. Dörnbrack, K, Kandler, L. Schütz, P. Knippertz, M. Fiebig, and A. Virkkula, 2008. Saharan dust refractive index and optical properties from aircraft-based observations during SAMUM 2006. *Tellus*, this issue.

Prospero, J.M., Long-range transport of mineral dust in the global atmosphere: Impact of African dust on environment of the southeastern United States, 1999. *Geology, Mineralogy, and Human welfare, colloquium paper,* 3396-3403.

Schladitz, A., T. Müller, A. Massling, N. Kaaden, K. Kandler, and A. Wiedensohler, 2008. In situ Measurements of Optical Properties at Tinfou (Morocco) during the Saharan Mineral Dust Experiment SAMUM 2006. *Tellus*, this issue.

Schepanski, K., I. Tegen, B. Laurent, B. Heinold, and A. Macke, 2007. A new Saharan dust source activation frequency map derived from MSG-SEVIRI IR channels.. *Geophys. Res. Lett. 34*, L18803, doi:10.1029/2007GL030168.

Von Hoyningen-Huene, W., T. Dinter, A.A. Kakhanovsky, J.P. Burrows, and M. Diouri, 2008. Measurements of desert dust optical characteristic at Porte au Sahara during SAMUM. *Tellus*, this issue.

Figure Captions

Figure 1. The 19 May 2006 SAMUM event. (a) MISR true-color nadir image of the Ouarzazate and Tinfou study sites and surrounding areas (Orbit 34136, Path 201). The latitudes, longitudes, and MISR Standard Product 558 nm AOT (Version 19) at the study sites are also given. (b) AEROENT multi-spectral AOT time series at Ouarzazate, and (c) Sun photometer multi-spectral AOT time series at Tinfou [*Dinter et al.*, 2008; *von Hoyningen-Huene et al.*, 2008], with the instantaneous 500 nm AOT at MISR overpass time (11:11 UTC) highlighted.

Figure 2. MISR Standard Aerosol Product (Version 19) results for the 19 May 2006 SAMUM event. (a) AOT at 558 nm. (b) Ångström Exponent, assessed by least-squared fit to the four MISR spectral bands that range from 446 to 867 nm. (c) Aerosol single-scattering albedo (SSA), assessed at 558 nm. (d) Fraction of 558 nm AOT retrieved as spherical particles. The region is about 380 km wide, and approximately 700 km along-track (MISR Blocks 64-68 of the standard product).

Figure 3. The 28 May 2006 SAMUM event. (a) MISR true-color nadir image of the Ouarzazate and Tinfou study sites and surrounding areas (Orbit 34267, Path 200). The MISR Standard Product 558 nm AOT (Version 19) at the study sites is also given. (b) AEROENT multi-spectral AOT time series at Ouarzazate, and (c) Sun photometer multi-spectral AOT time series at Tinfou, with the instantaneous 500 nm AOT at MISR overpass time (11:05 UTC) highlighted.

Figure 4. Same as Figure 2, but for the 28 May 2006 SAMUM event.

Figure 5. The 04 June 2006 SAMUM event. (a) MISR true-color nadir image of the Ouarzazate and Tinfou study sites and surrounding areas (Orbit 34369, Path 201). The MISR Standard Product 558 nm AOT (Version 19) at the study sites is also given. (b) AEROENT multi-spectral AOT time series at Ouarzazate, and (c) Sun photometer multi-spectral AOT time series at Tinfou, with the instantaneous 500 nm AOT at MISR overpass time (11:11 UTC) highlighted.

Figure 6. Same as Figure 2, but for the 04 June 2006 SAMUM event. The locations of a likely dust storm SSE of the prime study region and an apparent concentration of small, bright, spherical particles are marked in white, and the central latitudes and longitudes are given in parentheses.

Figure 7. Three-day back trajectories for the 04 June 2006 SAMUM event, evaluated at 1.8, 3, and 4 km above sea level from the HYSPLIT model [*Draxler and Rolph*, 2003] for (1) Ouarzazate, (2) Tinfou, and (3) near the center of the small, bright, spherical particle concentration of Figure 6.

Table 1. MISR Standard Aerosol Retrieval Algorithm (Version 19) Aerosol Components

Aerosol components are named based on particle shape (spherical, non-spherical grains, or spheroids), SSA (non-absorbing or absorbing), and number-weighted mean geometric radius (in μm). For absorbing aerosols, the green-band SSA is also given. This table lists the eight components used in Table 2.

Component #	Name/Description
1	spherical_nonabsorbing_0.06
2	spherical_nonabsorbing_0.12
3	spherical_nonabsorbing_0.26
6	spherical_nonabsorbing_2.80
8	spherical_absorbing_0.12_ssa_green_0.9
14	spherical_absorbing_0.12_ssa_green_0.8
19	medium_grains*
21	coarse_spheroids*

*A full description of the dust particle optical analogs used in the MISR Standard algorithm is given by *Kalashnikova et al.* [2005].

Table 2. MISR Standard Algorithm (Version 19) Aerosol Mixtures

Mixture	Component Fractional AOT (at 558 nm)								AOT rel. to green			Single Scattering Albedo			
#	1*	2*	3*	6*	8*	14*	19*	21*	blue	red	nir	blue	green	red	nir
1	1	-	-	-	-	-	-	-	1.95	0.549	0.23	1	1	1	1
2	0.95	-	-	0.05	-	-	-	-	1.9	0.573	0.271	1	1	1	1
3	0.9	-	-	0.1	-	-	-	-	1.85	0.596	0.312	1	1	1	1
4	0.8	-	-	0.2	-	-	-	-	1.76	0.644	0.395	1	1	1	1
5	0.7	-	-	0.3	-	-	-	-	1.66	0.691	0.477	1	1	1	1
6	0.6	-	-	0.4	-	-	-	-	1.57	0.738	0.559	1	1	1	1
7	0.5	-	-	0.5	-	-	-	-	1.47	0.786	0.642	1	1	1	1
8	0.4	-	-	0.6	-	-	-	-	1.37	0.833	0.724	1	1	1	1
9	0.3	-	-	0.7	-	-	-	-	1.28	0.881	0.807	1	1	1	1
10	0.2	-	-	0.8	-	-	-	-	1.18	0.928	0.889	1	1	1	1
11	-	1	-	-	-	-	-	-	1.54	0.66	0.348	1	1	1	1
12	-	0.95	-	0.05	-	-	-	-	1.51	0.679	0.384	1	1	1	1
13	-	0.9	-	0.1	-	-	-	-	1.49	0.697	0.419	1	1	1	1
14	-	0.8	-	0.2	-	-	-	-	1.43	0.733	0.49	1	1	1	1
15	-	0.7	-	0.3	-	-	-	-	1.38	0.769	0.56	1	1	1	1
16	-	0.6	-	0.4	-	-	-	-	1.32	0.805	0.631	1	1	1	1
17	-	0.5	-	0.5	-	-	-	-	1.26	0.842	0.701	1	1	1	1
18	-	0.4	-	0.6	-	-	-	-	1.21	0.878	0.772	1	1	1	1
19	-	0.3	-	0.7	-	-	-	-	1.15	0.914	0.843	1	1	1	1
20	-	0.2	-	0.8	-	-	-	-	1.1	0.95	0.913	1	1	1	1
21	-	-	1	-	-	-	-	-	1.18	0.82	0.576	1	1	1	1
22	-	-	0.95	0.05	-	-	-	-	1.17	0.83	0.6	1	1	1	1
23	-	-	0.9	0.1	-	-	-	-	1.17	0.841	0.624	1	1	1	1
24	-	-	0.8	0.2	-	-	-	-	1.15	0.861	0.672	1	1	1	1
25	-	-	0.7	0.3	-	-	-	-	1.13	0.881	0.72	1	1	1	1

26	-	-	0.6	0.4	-	-	-	-	1.11	0.901	0.767	1	1	1	1
27	-	-	0.5	0.5	-	-	-	-	1.09	0.921	0.815	1	1	1	1
28	-	-	0.4	0.6	-	-	-	-	1.07	0.942	0.863	1	1	1	1
29	-	-	0.3	0.7	-	-	-	-	1.05	0.962	0.911	1	1	1	1
30	-	-	0.2	0.8	-	-	-	-	1.03	0.982	0.959	1	1	1	1
31	-	-	-	-	1	-	-	-	1.51	0.677	0.375	0.911	0.9	0.885	0.8
32	-	-	-	0.05	0.95	-	-	-	1.48	0.694	0.409	0.914	0.905	0.894	0.8
33	-	-	-	0.1	0.9	-	-	-	1.45	0.712	0.443	0.917	0.91	0.902	0.8
34	-	-	-	0.2	0.8	-	-	-	1.4	0.746	0.511	0.924	0.92	0.917	0.9
35	-	-	-	0.3	0.7	-	-	-	1.35	0.781	0.578	0.931	0.93	0.93	0.9
36	-	-	-	0.4	0.6	-	-	-	1.3	0.815	0.646	0.938	0.94	0.943	0.9
37	-	-	-	0.5	0.5	-	-	-	1.25	0.85	0.714	0.946	0.95	0.954	0.9
38	-	-	-	0.6	0.4	-	-	-	1.2	0.884	0.782	0.955	0.96	0.965	0.9
39	-	-	-	0.7	0.3	-	-	-	1.14	0.919	0.85	0.965	0.97	0.975	0.9
40	-	-	-	0.8	0.2	-	-	-	1.09	0.953	0.918	0.976	0.98	0.984	0.9
41	-	-	-	-	-	1	-	-	1.47	0.695	0.403	0.821	0.8	0.773	0.7
42	-	-	-	0.05	-	0.95	-	-	1.45	0.712	0.436	0.827	0.81	0.79	0.7
43	-	-	-	0.1	-	0.9	-	-	1.42	0.728	0.468	0.833	0.82	0.805	0.7
44	-	-	-	0.2	-	0.8	-	-	1.37	0.761	0.533	0.847	0.84	0.834	0.8
45	-	-	-	0.3	-	0.7	-	-	1.33	0.793	0.598	0.861	0.86	0.861	0.8
46	-	-	-	0.4	-	0.6	-	-	1.28	0.826	0.664	0.876	0.88	0.886	0.8
47	-	-	-	0.5	-	0.5	-	-	1.23	0.859	0.729	0.893	0.9	0.908	0.9
48	-	-	-	0.6	-	0.4	-	-	1.18	0.892	0.794	0.911	0.92	0.929	0.9
49	-	-	-	0.7	-	0.3	-	-	1.13	0.924	0.859	0.93	0.94	0.949	0.9
50	-	-	-	0.8	-	0.2	-	-	1.08	0.957	0.924	0.952	0.96	0.967	0.9
51	-	0.72	-	0.08	-	-	0.2	-	1.37	0.77	0.551	0.989	0.995	0.998	0.9
52	-	0.48	-	0.32	-	-	0.2	-	1.24	0.857	0.72	0.988	0.995	0.999	0.9
53	-	0.16	-	0.64	-	-	0.2	-	1.06	0.973	0.946	0.986	0.995	0.999	0.9
54	-	0.54	-	0.06	-	-	0.4	-	1.25	0.844	0.683	0.977	0.991	0.997	0.9
55	-	0.36	-	0.24	-	-	0.4	-	1.15	0.909	0.81	0.975	0.991	0.997	0.9
56	-	0.12	-	0.48	-	-	0.4	-	1.02	0.996	0.979	0.972	0.991	0.998	0.9
57	-	0.36	-	0.04	-	-	0.6	-	1.13	0.918	0.815	0.962	0.986	0.996	0.9
58	-	0.24	-	0.16	-	-	0.6	-	1.07	0.961	0.9	0.959	0.986	0.996	0.9
59	-	0.08	-	0.32	-	-	0.6	-	0.977	1.02	1.01	0.956	0.986	0.997	0.9
60	-	0.18	-	0.02	-	-	0.8	-	1.01	0.991	0.947	0.943	0.982	0.995	0.9
61	-	0.12	-	0.08	-	-	0.8	-	0.98	1.01	0.989	0.941	0.982	0.995	0.9
62	-	0.04	-	0.16	-	-	0.8	-	0.936	1.04	1.05	0.938	0.982	0.995	0.9
63	-	0.4	-	-	-	-	0.48	0.12	1.16	0.898	0.783	0.951	0.977	0.993	0.9
64	-	0.4	-	-	-	-	0.36	0.24	1.18	0.892	0.78	0.94	0.968	0.99	0.9
65	-	0.4	-	-	-	-	0.24	0.36	1.19	0.887	0.776	0.928	0.959	0.986	0.9
66	-	0.4	-	-	-	-	0.12	0.48	1.2	0.881	0.773	0.918	0.95	0.983	0.9
67	-	0.2	-	-	-	-	0.64	0.16	1.04	0.977	0.928	0.927	0.97	0.991	0.9
68	-	0.2	-	-	-	-	0.48	0.32	1.05	0.969	0.924	0.91	0.958	0.987	0.9
69	-	0.2	-	-	-	-	0.32	0.48	1.07	0.962	0.919	0.894	0.946	0.983	0.9
70	-	0.2	-	-	-	-	0.16	0.64	1.08	0.954	0.914	0.879	0.934	0.979	0.9
71	-	-	-	-	-	-	0.8	0.2	0.914	1.06	1.07	0.896	0.962	0.99	0.9
72	-	-	-	-	-	-	0.6	0.4	0.933	1.05	1.07	0.873	0.947	0.985	0.9
73	-	-	-	-	-	-	0.4	0.6	0.951	1.04	1.06	0.851	0.932	0.98	0.9
74	-	-	-	-	-	-	0.2	0.8	0.97	1.03	1.06	0.83	0.917	0.976	0.9

* The eight components used in this mixture table are described in Table 1.

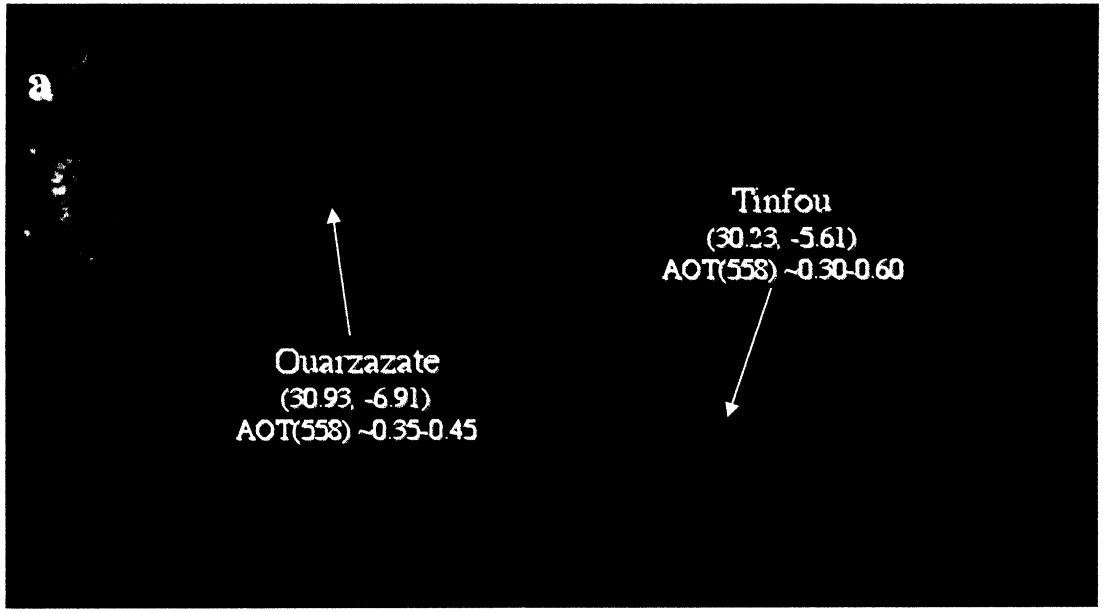
a
Tinfou
(30.23, -5.61)
AOT(558) ~0.30-0.60
Ouarzazate
(30.93, -6.91)
AOT(558) ~0.35-0.45

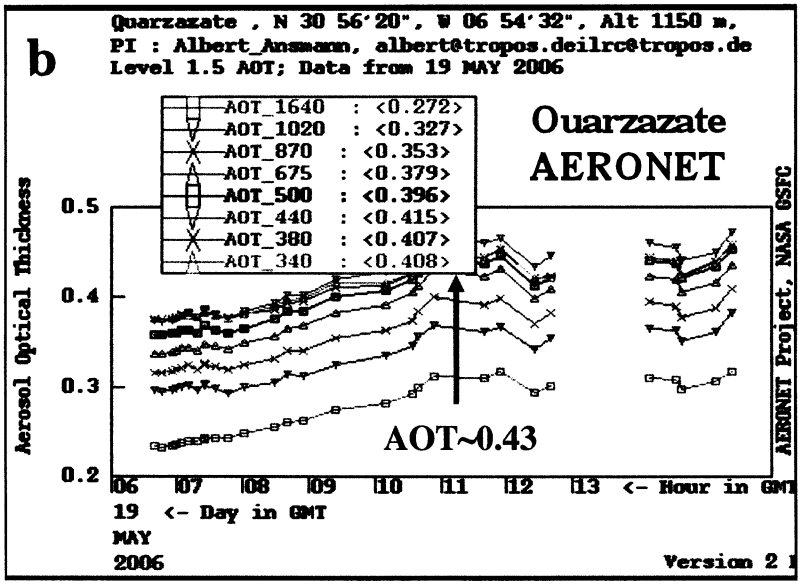
b
Quarzazate , N 30 56'20", W 06 54'32", Alt 1150 m,
PI : Albert_Ansmann, albert@tropos.deilrc@tropos.de
Level 1.5 AOT; Data from 19 MAY 2006
AOT_1640 : <0.272>
AOT_1020 : <0.327>
AOT_870 : <0.353>
AOT_675 : <0.379>
AOT_500 : <0.396>
AOT_440 : <0.415>
AOT_380 : <0.407>
AOT_340 : <0.408>
Ouarzazate
AERONET
Aerosol Optical Thickness
0.5
0.4
0.3
0.2
AOT~0.43
06 07 08 09 10 11 12 13 <- Hour in GMT
19 <- Day in GMT
MAY
2006
AERONET Project, NASA GSFC
Version 2

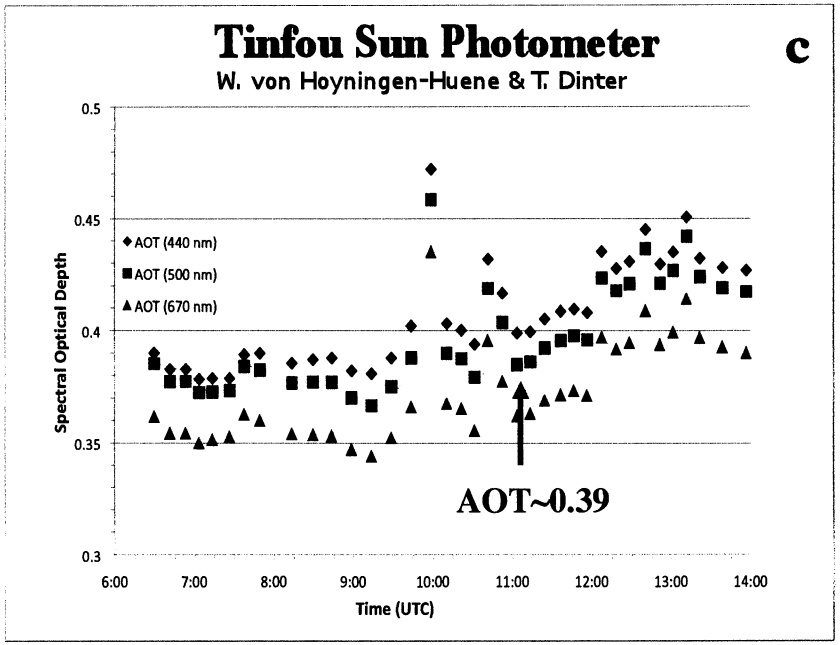
Tinfou Sun Photometer
W. von Hoyningen-Huene & T. Dinter
c
Spectral Optical Depth
0.5
0.45
0.4
0.35
0.3
AOT (440 nm)
AOT (500 nm)
AOT (670 nm)
AOT~0.39
6:00 7:00 8:00 9:00 10:00 11:00 12:00 13:00 14:00
Time (UTC)

Figure 1

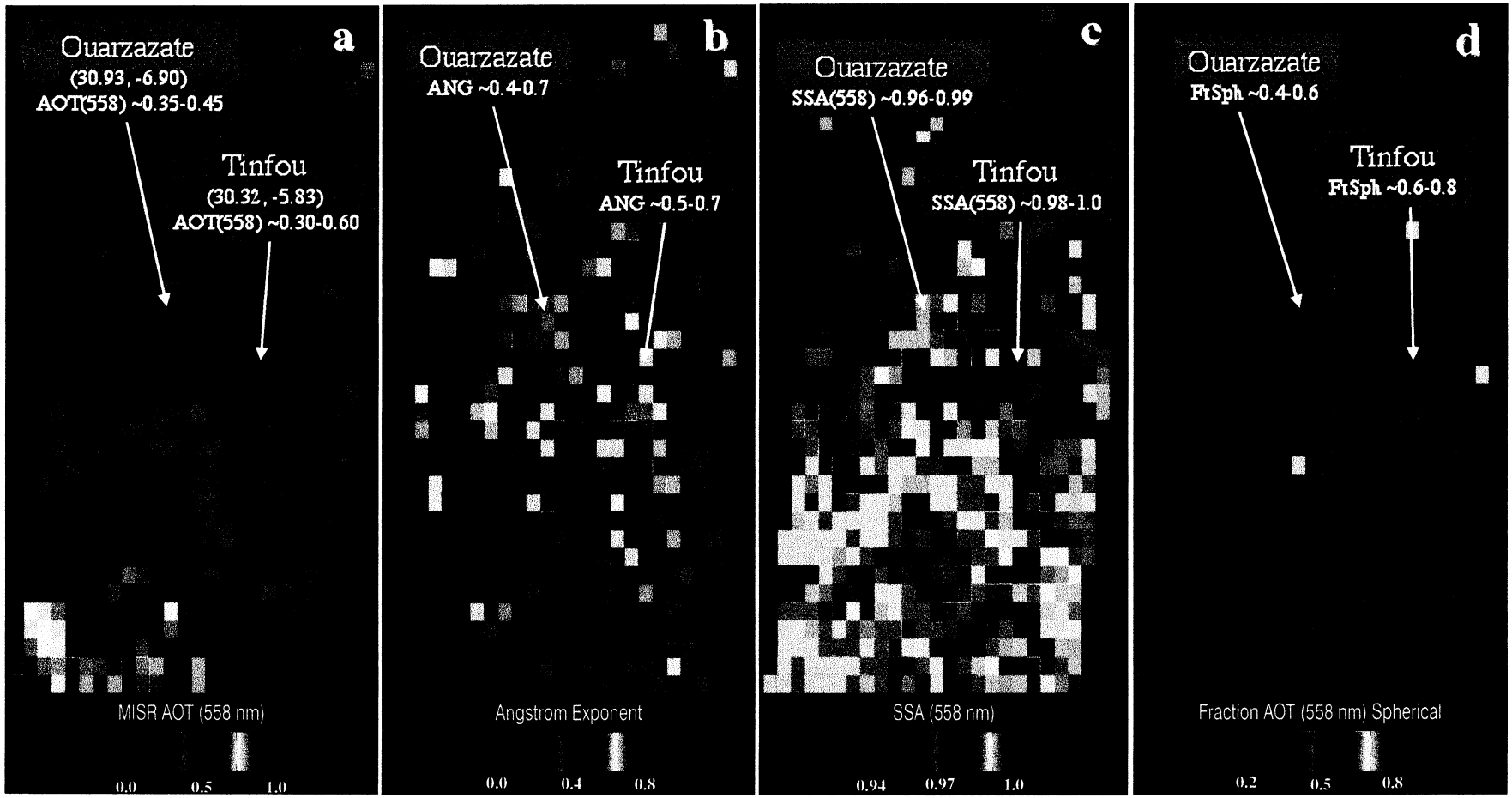
a
Ouarzazate
(30.93, -6.90)
AOT(558) ~0.35-0.45
Tinfou
(30.32, -5.83)
AOT(558) ~0.30-0.60
MISR AOT (558 nm)
0.0
0.5
1.0
b
Ouarzazate
ANG ~0.4-0.7
Tinfou
ANG ~0.5-0.7
Angstrom Exponent
0.0
0.4
0.8
c
Ouarzazate
SSA(558) ~0.96-0.99
Tinfou
SSA(558) ~0.98-1.0
SSA (558 nm)
0.94
0.97
1.0
d
Ouarzazate
FrSph ~0.4-0.6
Tinfou
FrSph ~0.6-0.8
Fraction AOT (558 nm) Spherical
0.2
0.5
0.8

Figure 2

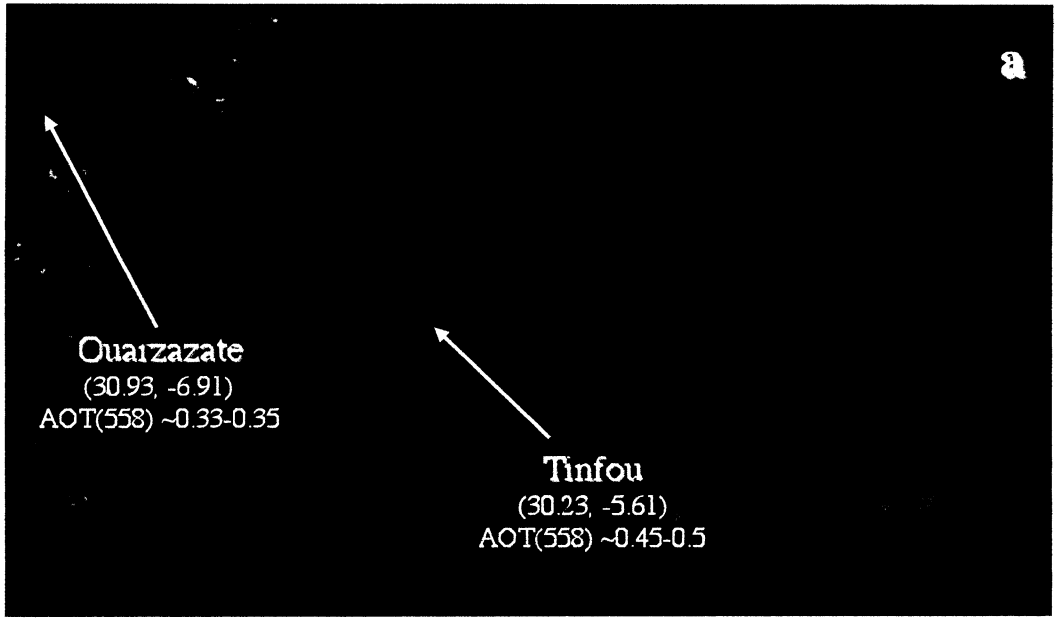
a
Ouarzazate
(30.93, -6.91)
AOT(558) ~0.33-0.35
Tinfou
(30.23, -5.61)
AOT(558) ~0.45-0.5

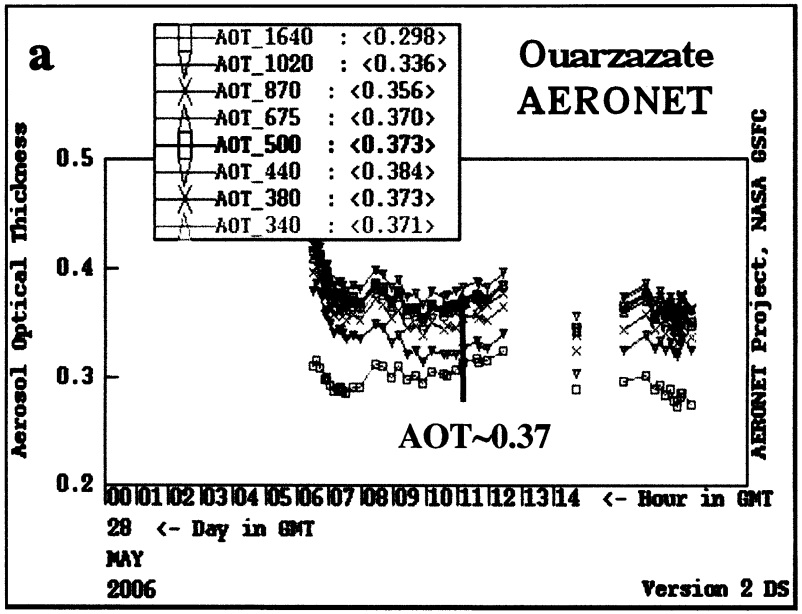
a
AOT_1640 : <0.298>
AOT_1020 : <0.336>
AOT_870 : <0.356>
AOT_675 : <0.370>
AOT_500 : <0.373>
AOT_440 : <0.384>
AOT_380 : <0.373>
AOT_340 : <0.371>
Ouarzazate
AERONET
Aerosol Optical Thickness
0.5
0.4
0.3
0.2
AOT~0.37
AERONET Project, NASA GSFC
00 01 02 03 04 05 06 07 08 09 10 11 12 13 14 <- Hour in GMT
28 <- Day in GMT
MAY
2006
Version 2 DS

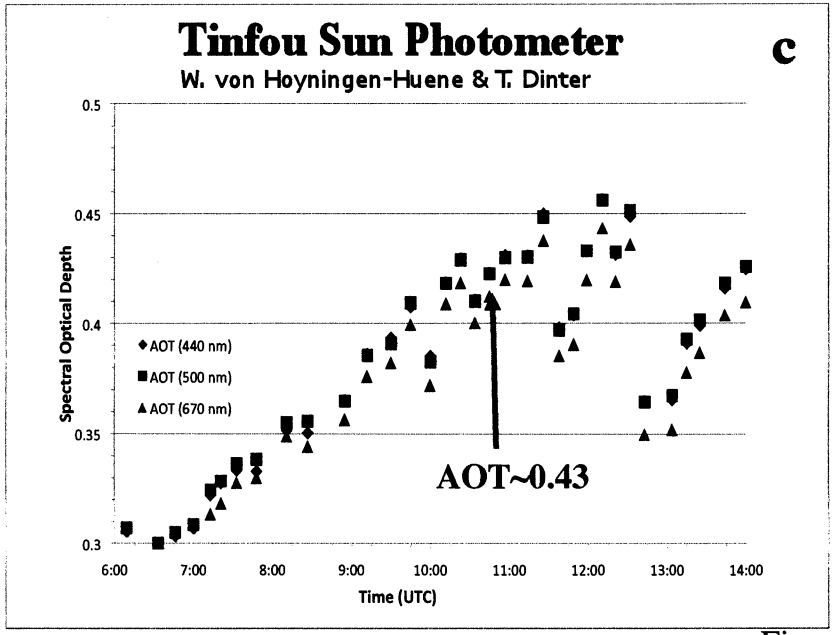
Tinfou Sun Photometer
W. von Hoyningen-Huene & T. Dinter
c
Spectral Optical Depth
0.5
0.45
0.4
0.35
0.3
AOT (440 nm)
AOT (500 nm)
AOT (670 nm)
AOT~0.43
6:00
7:00
8:00
9:00
10:00
11:00
12:00
13:00
14:00
Time (UTC)

Figure 3

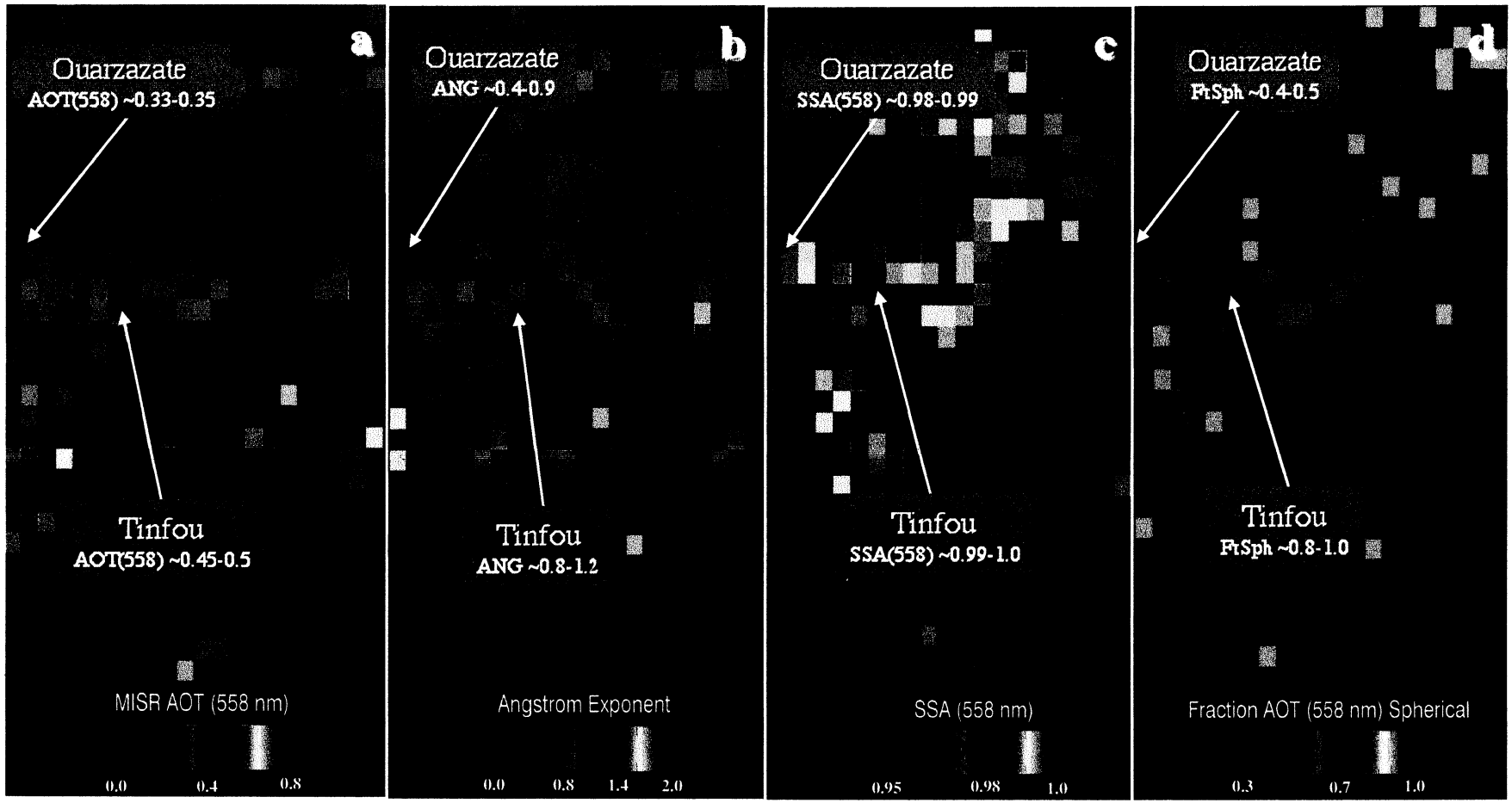
a
Ouarzazate
AOT(558) ~0.33-0.35
Tinfou
AOT(558) ~0.45-0.5
MISR AOT (558 nm)
0.0
0.4
0.8
b
Ouarzazate
ANG ~0.4-0.9
Tinfou
ANG ~0.8-1.2
Angstrom Exponent
0.0
0.8
1.4
2.0
c
Ouarzazate
SSA(558) ~0.98-0.99
Tinfou
SSA(558) ~0.99-1.0
SSA (558 nm)
0.95
0.98
1.0
d
Ouarzazate
FtSph ~0.4-0.5
Tinfou
FtSph ~0.8-1.0
Fraction AOT (558 nm) Spherical
0.3
0.7
1.0

Figure 4

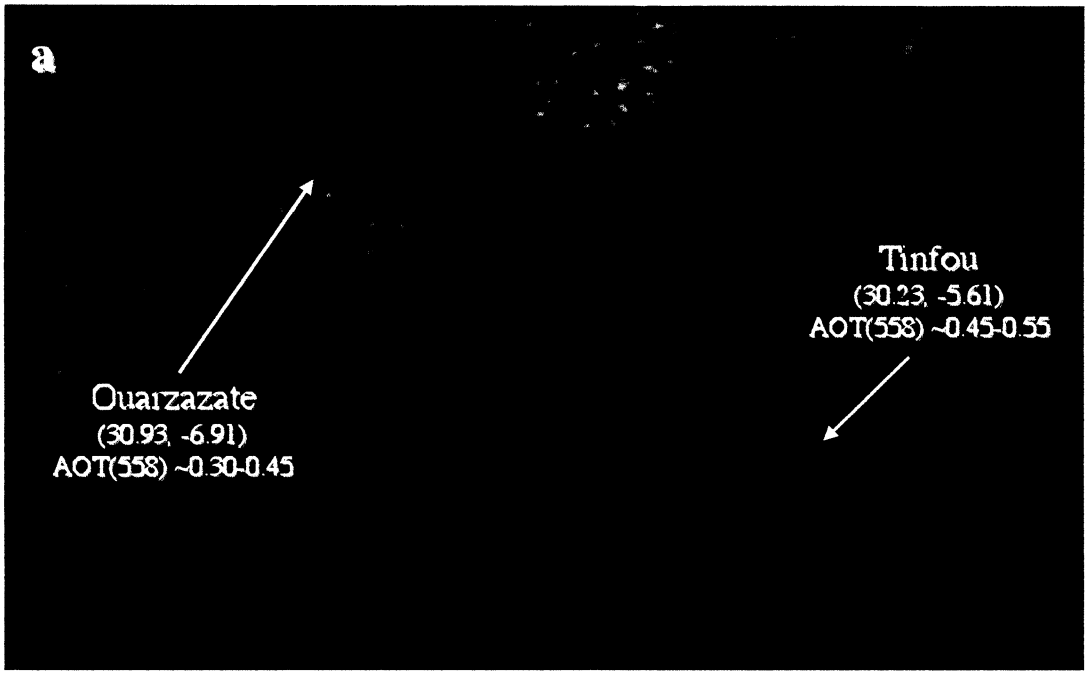
a
Tinfou
(30.23, -5.61)
AOT(558) ~0.45-0.55
Ouarzazate
(30.93, -6.91)
AOT(558) ~0.30-0.45

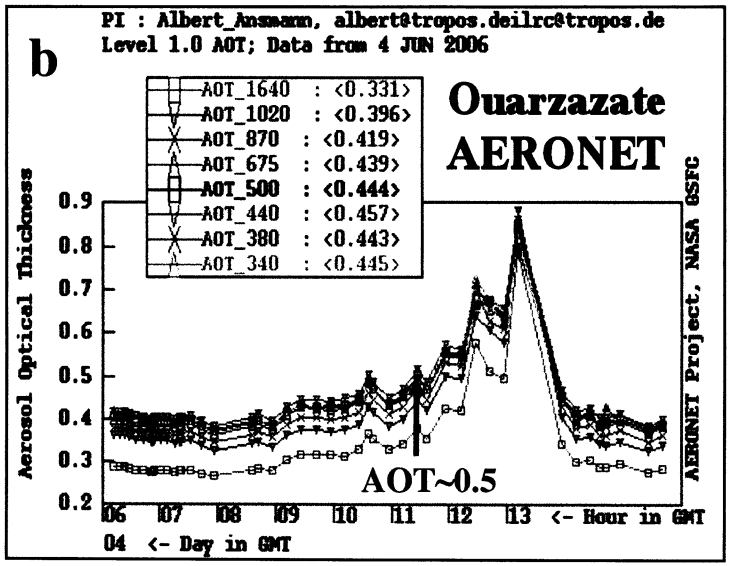
b
PI : Albert_Ansmann, albert@tropos.deilrc@tropos.de
Level 1.0 AOT; Data from 4 JUN 2006
AOT_1640 : <0.331>
AOT_1020 : <0.396>
AOT_870 : <0.419>
AOT_675 : <0.439>
AOT_500 : <0.444>
AOT_440 : <0.457>
AOT_380 : <0.443>
AOT_340 : <0.445>
Ouarzazate
AERONET
Aerosol Optical Thickness
AERONET Project, NASA GSFC
AOT~0.5
06 07 08 09 10 11 12 13 <- Hour in GMT
04 <- Day in GMT

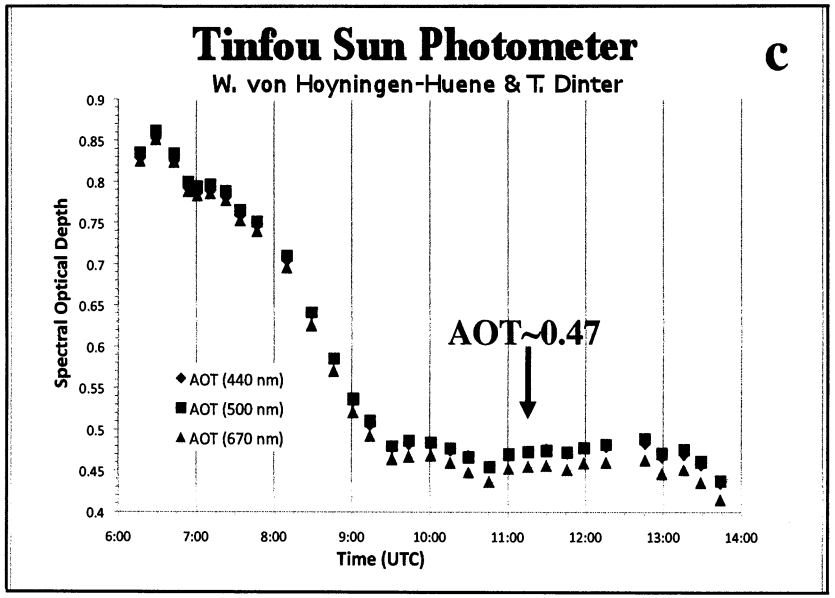
Tinfou Sun Photometer
c
W. von Hoyningen-Huene & T. Dinter
Spectral Optical Depth
AOT (440 nm)
AOT (500 nm)
AOT (670 nm)
AOT~0.47
Time (UTC)

Figure 5

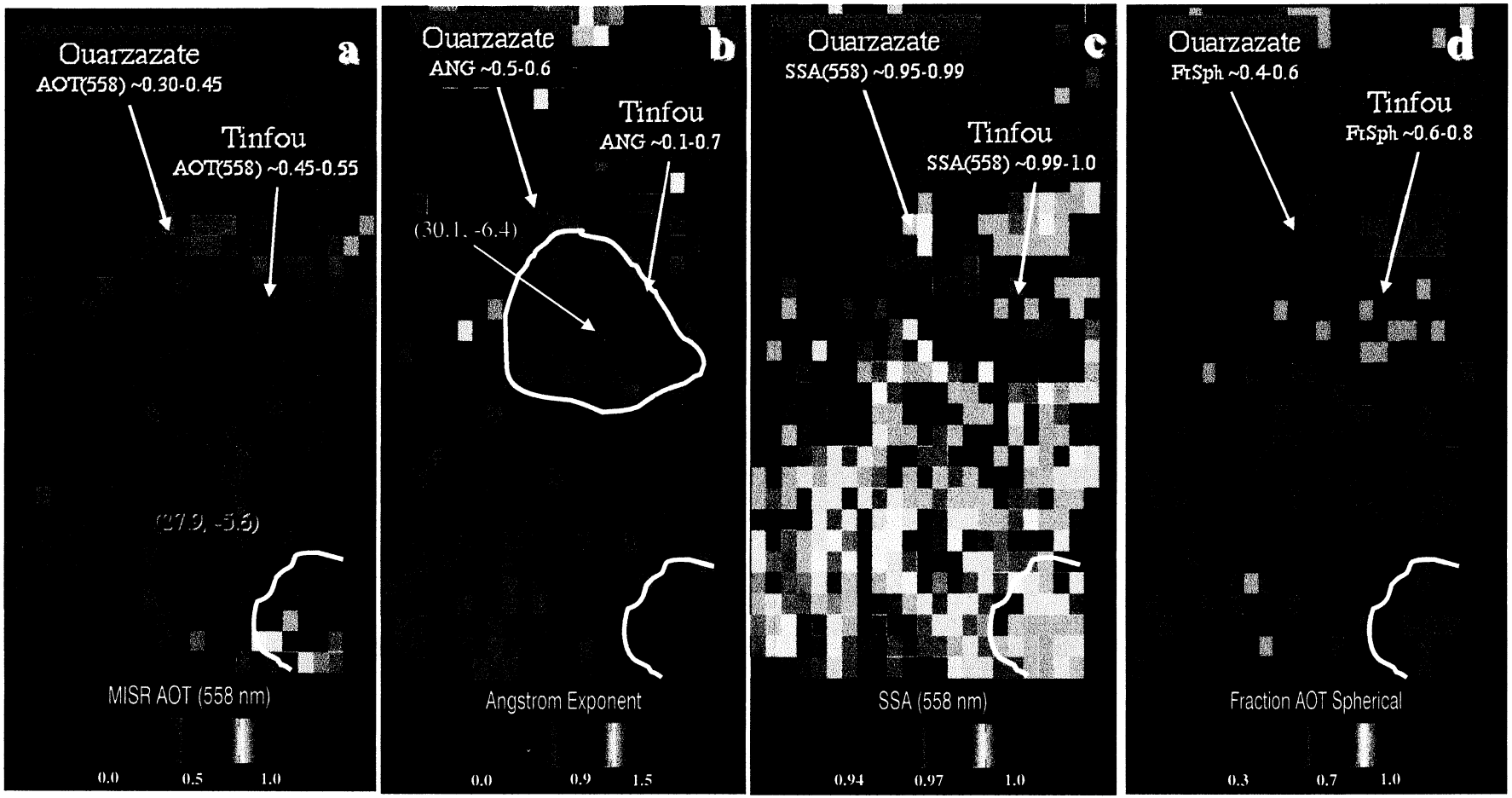
Ouarzazate
AOT(558) ~0.30-0.45
a
Tinfou
AOT(558) ~0.45-0.55
(27.9, -5.5)
MISR AOT (558 nm)
0.0
0.5
1.0
Ouarzazate
ANG ~0.5-0.6
b
Tinfou
ANG ~0.1-0.7
(30.1, -6.4)
Angstrom Exponent
0.0
0.9
1.5
Ouarzazate
SSA(558) ~0.95-0.99
c
Tinfou
SSA(558) ~0.99-1.0
SSA (558 nm)
0.94
0.97
1.0
Ouarzazate
FrSph ~0.4-0.6
d
Tinfou
FrSph ~0.6-0.8
Fraction AOT Spherical
0.3
0.7
1.0

Figure 6

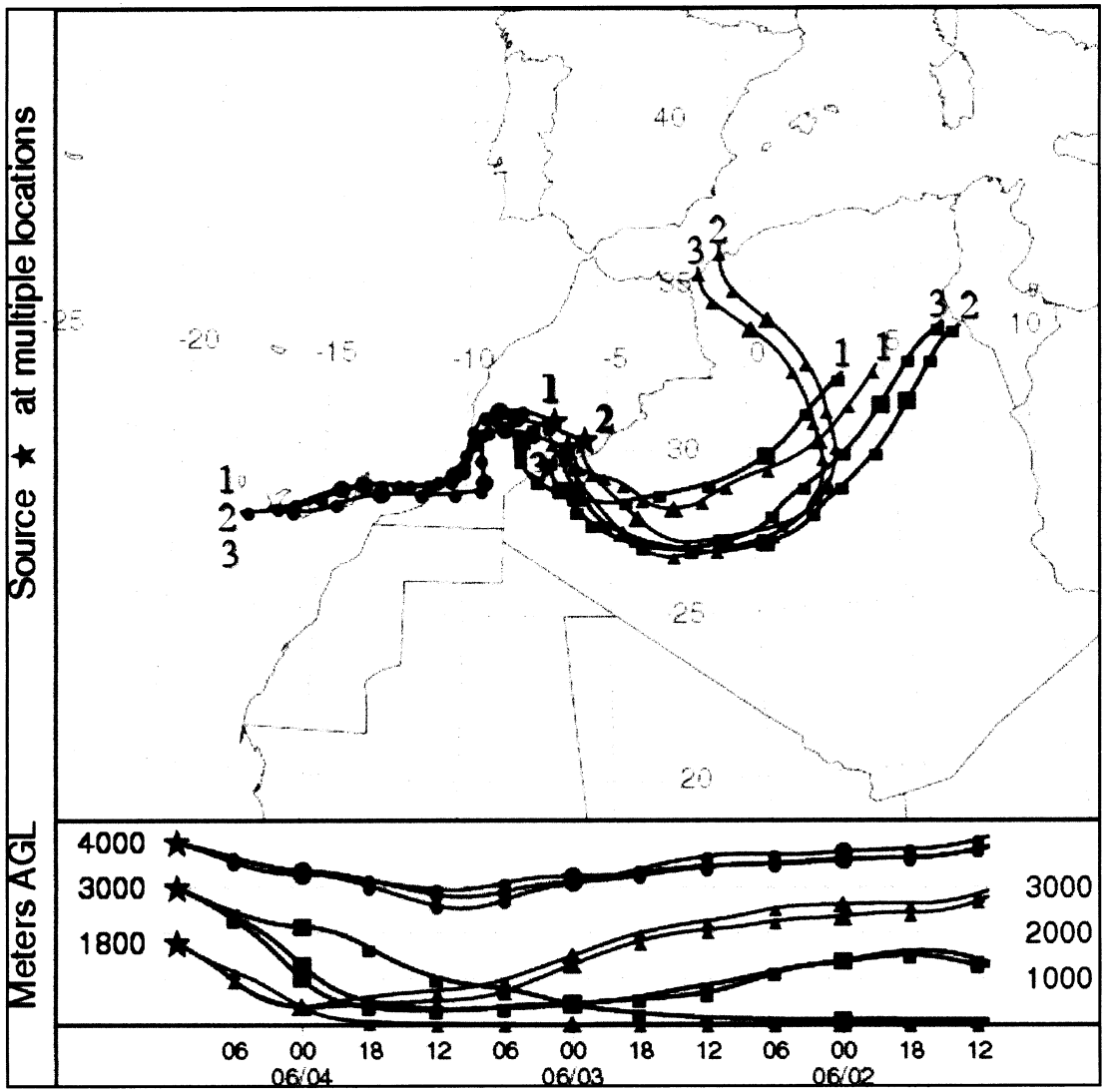
Source ★ at multiple locations
Meters AGL
4000
3000
1800
3000
2000
1000
06 00 18 12 06 00 18 12 06 00 18 12
06/04
06/03
06/02

Figure 7